Progress in Nuclear Energy 92 (2016) 91–103

Contents lists available at ScienceDirect

Progress in Nuclear Energy

journal homepage: www.elsevier.com/locate/pnucene

A point kinetics model for dynamic simulations of next generation nuclear reactor

Mohamed S. El-Genk [a, b, c, d, *], Jean-Michel P. Tournier [a]

[a] Institute for Space and Nuclear Power Studies, The University of New Mexico, Albuquerque, NM, USA
[b] Nuclear Engineering Department, The University of New Mexico, Albuquerque, NM, USA
[c] Mechanical Engineering Department, The University of New Mexico, Albuquerque, NM, USA
[d] Chemical and Biological Engineering Department, The University of New Mexico, Albuquerque, NM, USA

ARTICLE INFO

Article history:
Received 25 May 2016
Received in revised form
5 July 2016
Accepted 7 July 2016
Available online 22 July 2016

Keywords:
Six-group point kinetics
Dynamic simulation
Next generation nuclear reactor
High temperature reactor
Prompt jump approximation
Padé(3,3) function
Simulation transients

ABSTRACT

An accurate, fast-running and stable six-group, point kinetics (PK) model is developed and applied successfully to the dynamic simulation of the operation of the prismatic core, high temperature next generation nuclear plant (NGNP) reactor. The model is unrestricted by the size of the time step, which could be as much as several seconds, accounts for Doppler Broadening and the fuel and graphite temperature reactivity feedbacks, and includes an active neutron source for zero-power reactor startup. An efficient and robust numerical technique that approximates the exponential matrix using 7th order-accurate Padé(3,3) function with a discretization error on the order of $(\Delta t)^3$, solves the coupled nonlinear and stiff six-groups point kinetics equations. The PK model handles reactivity insertions in excess of a prompt critical, $\rho/\overline{\beta}>$ \$1.0, with unrestrictive time step size. Model results are successfully benchmarked using the Inhour solution for a step insertion of external reactivity. To simulate the transient response of the NGNP reactor following an external reactivity insertion and during a startup, the PK model is coupled to 84-nodes thermal-hydraulics model of the reactor, also developed in this work. With a 2 s time step, the error of predicting the reactor thermal power is ~0.001%, increasing exponentially to ~0.08% and ~1.5% with increased time step size to 5 and 8 s, respectively. The present PK model has been successfully incorporated into MELCOR-H_2 nuclear reactor analysis code to simulate transient operation of Very High Temperature Reactor (VHTR) for electricity generation, using a Closed Brayton Cycle turbomachinery, and the co-generation of hydrogen using Sulfur Iodine (SI) thermochemical processes.

1. Introduction

The Next Generation Nuclear Plant (NGNP) project was established in 2005 by United States Department of Energy (DOE), as required by Congress in Subtitle C of Title VI of the Energy Policy Act. The objective was to develop, license, build, and operate a prototype modular high temperature helium gas-cooled reactor (HTGR) plant for electricity generation at high thermal efficiency > 45%, the cogeneration of hydrogen using thermochemical processes, and the co-production of high-temperature process heat for energy-intensive industrial uses. The pre-licensing interactions for the NGNP began in 2006 and were suspended in 2013 after DOE decided in 2011 to cease detailed design and license application phases, citing impasses with the NGNP Industry Alliance on cost sharing arrangements for the public-private partnership required by Congress. Nonetheless, design development and construction activities of HTGRs for commercial applications continued in many countries around the world, notably China (Zhang et al., 2009). Licensing these reactors require developing and validating system codes, such as RELAP5-3D and MELCOR-H2, with transient analysis capabilities (Gauntt et al., 2000; Rodriguez et al., 2007; RELAP5-3D© Code Development RELAP5-3D Code Development Team, 2012). Due to the complexity of these codes, the time step for the transient simulations should not be restricted by the stability and accuracy of the solution of the reactor's six-group point kinetics equations.

In order to assess the effects of certain operation transients on the neutronics and thermal hydraulics parameters, and the

* Corresponding author. Founding Director, Institute for Space and Nuclear Power Studies, The University of New Mexico, USA.
E-mail address: mgenk@unm.edu (M.S. El-Genk).

http://dx.doi.org/10.1016/j.pnucene.2016.07.007
0149-1970/

performance of a nuclear reactor, it is desirable to demonstrate robust capabilities for simulating these transients and performing complex safety analyses. This would require solving the six-group point kinetics equations, with the applicable reactivity feedback effects, as a function of space and time and integrating the solution in a system analyses code such as MELCO-H2 (Rodriguez et al., 2007, 2009) and RELAP5-3D (RELAP5-3D© Code Development RELAP5-3D Code Development Team, 2012). Such an approach is quite complex and would require huge computational capabilities.

An alternative approach couples the reactor thermal-hydraulics (TH) to the solution of the reactor's nonlinear point kinetics (PK) equations, with applicable values of the reactivity feedbacks, the neutron lifetime, and the concentrations and decay constants of the delayed neutron groups. These values are determined from separate neutronics analyses of the reactor type of interest. This approach is more practical and efficient to incorporate into large system codes, such as RELAP5-3D (RELAP5-3D© Code Development RELAP5-3D Code Development Team, 2012) and MELCOR-H2 (Rodriguez et al., 2007), but the time step for solving the point kinetics equations needs to be much less restrictive than that used by the thermal-hydraulics and safety analysis models in the codes.

The six-group point kinetics equations are a set of transient, stiff, nonlinear and coupled ordinary differential equations for calculating the fission power and the concentrations of the delayed neutron groups or precursors, in response to changes in the reactor temperatures and/or an external reactivity insertion during a reactor startup and following a reactivity insertion or a change in the operating thermal power of the reactor. For representative results, the values of the delayed neutron concentrations and decay constants, the neutron generation life time, and the various temperature reactivity feedbacks for the fuel, moderator, and coolant, and due to Doppler broadening need to be determined and incorporated into the solution of the point kinetics equations.

Numerous approximate analytical and numerical solutions of the point kinetics equations have been reported (Kinard and Allen, 2004; Quintero-Leyva, 2008; Nahla and Zayed, 2010; Mamieh and Saidinezhad, 2012). They are either oversimplified, to speed up the transient analyses of nuclear reactors and/or require using a very small time steps for accuracy and solution stability. Recently, Ganapol (2013) has introduced a unique contribution to solving the PK equations using a semi-analytical method, based on a piecewise constant approximation and accounting for the reactivity feedback effect. The demonstrated results were quite accurate for a time step of as large as 0.01s.

The objective of this paper is to develop an accurate, fast-running and stable 6-point kinetics model for simulating the transient response of the prismatic core, high temperature NGNP reactor (MacDonald et al., 2003), with unrestrictive time step size. The developed point kinetics (PK) model accounts for the effects of Doppler broadening and the fuel and graphite temperature reactivity feedbacks, and includes an active neutron source for zero-power reactor startup. The coupled six-groups point kinetics equations are solved using an efficient methodology that approximates the exponential matrix using 7th order-accurate Padé(3,3) function, with a discretization error on the order of $(\Delta t)^3$ and an unrestrictive time step. The PK model results are successfully benchmarked using those of the Inhour analytical solution for step reactivity insertions in excess of a prompt critical, $\rho/\overline{\beta} > \$1.0$.

To simulate the transient response of the NGNP reactor, following an external reactivity insertion and during a reactor startup, the PK model is coupled to 84-nodes thermal-hydraulics model of the NGNP reactor. The PK model detailed in this paper has been incorporated into the MELCOR-H_2 nuclear reactor analysis code (Rodriguez et al., 2007, 2009) to simulate operation transients of Very High Temperature Reactor (VHTR), for electricity generation, using a closed Brayton Cycle turbomachinery, and the co-generation of hydrogen using Sulfur Iodine (SI) thermochemical processes. This PK model could also be applied to other reactor types, after incorporating the applicable reactivity feedbacks and kinetics parameters.

1.1. Point kinetics equations

The governing equations in the present PK model are expressed in terms of the reactor's thermal power, P, and the delayed-neutron precursors, $\{Y_i\}$, as:

$$\frac{dP}{dt} = \frac{\rho - \overline{\beta}}{\Lambda} \times P + \sum_{i=1}^{6} \lambda_i Y_i + S_o, \tag{1}$$

$$\frac{dY_i}{dt} = \frac{\beta_i}{\Lambda} \times P - \lambda_i Y_i, \quad \text{i} = 1 \text{ to } 6. \tag{2}$$

The total reactivity, ρ, is expressed in terms of the effective multiplication factor, k, as:

$$\rho = \frac{k-1}{k} = 1 - \frac{1}{k}. \tag{3}$$

The neutron generation time(s), $\Lambda = (\nu\nu\Sigma_f)^{-1}$, and the thermal power (W) generated by the ith group of the delayed-neutron precursors is given as:

$$Y_i = Q_f VOL \times \frac{C_i(t)}{\nu\Lambda}, \tag{4}$$

The rate of thermal power generation by the active neutron source (W/s) in Equation (1) is expressed as:

$$S_o = Q_f \times \frac{s'_o}{\nu\Lambda}. \tag{5}$$

The coupled set of stiff and nonlinear, first-order differential equations (1) and (2), is solved subject to the initial conditions:

$$P_{(t=0)} = P_o, \; Y_{i(t=0)} = Y_i^o, \text{ where i} = 1 \text{ to } 6. \tag{6}$$

Assuming an initial equilibrium at $t = 0$, then$dY_i/dt = 0$, where $i = 1$ to 6, and$(dP/dt) = 0$, reducing Equation (2) to simple form:

$$Y_{i(t=0)} = Y_i^o = \frac{\beta_i}{\lambda_i \Lambda} P_o, \text{ where i} = 1 \text{ to } 6. \tag{7}$$

When an active neutron source is present ($s'_o > 0$), a small negative external reactivity, $\rho_o < 0$, needs to be inserted in equation (1) to ensure equilibrium, thus:

$$\rho_o = -\frac{\Lambda S_o}{P_o}. \tag{8}$$

With no active source present ($s'_o = 0$), a zero external reactivity, $\rho_o = 0$, ensures equilibrium. In this case, the reactor becomes critical at any thermal power, P_o, where those powers generated by delayed neutron precursors are related to P_o by Equation (7). For transients simulations of the NGNP reactor, the total reactivity in Equation (1), ρ, is the sum of the external reactivity, ρ_{ext} (active control), and the fuel Doppler reactivity feedback, ρ_D, the fuel temperature reactivity feedback, ρ_f, and the graphite temperature reactivity feedback, ρ_G, thus:

$$\rho = \rho_{ext} + \rho_D + \rho_f + \rho_G. \tag{9}$$

1.2. Temperature reactivity feedbacks

Expressions for the different feedback reactivity in Equation (9) are derived from the least-square fits of neutronics results of the NGNP prismatic reactor (MacDonald et al., 2003). The reported results (Fig. 1) are for: (a) the effective reactor multiplication factor, k, with a constant and uniform fuel temperature, $T_f = 1373$ K, and variable, but uniform graphite moderator/reflector temperatures; (b) the effective reactor multiplication factor, k, for a constant and uniform graphite temperature, $T_G = 1200$ K, and variable but uniform fuel temperatures; and (c) the effective reactor multiplication factor, k, for an isothermal core condition ($T_f = T_G$).

For the NGNP reactor, the calculated values of the temperature reactivity feedbacks (MacDonald et al., 2003) are expressed in terms of the volume-averaged fuel and graphite moderator/reflector temperatures, $\overline{T}_f$ and $\overline{T}_G$. The values for the fuel Doppler reactivity feedback (Fig. 1) are well correlated using a logarithmic function, as:

$$\rho_D = \chi_D \ln\left(\overline{T}_f \big/ T_f^o\right). \tag{10}$$

The fuel temperature reactivity feedback is best fit (Fig. 1) using a 2nd order polynomial of the volume-averaged fuel temperature, as:

$$\rho_f = \chi_{f,1}\left(\overline{T}_f - T_f^o\right) + \chi_{f,2}\left[\left(\overline{T}_f\right)^2 - \left(T_f^o\right)^2\right]. \tag{11}$$

The graphite temperature reactivity feedback is fit best (Fig. 1) using a 4th order polynomial of its volume-averaged temperature, as:

$$\rho_G = \sum_{m=1}^{4} \chi_{G,m}\left[\left(\overline{T}_G\right)^m - \left(T_G^o\right)^m\right]. \tag{12}$$

The coefficients χ_j, in Equations (10)–(12), determined from the least-squared fits of the reported calculations by MacDonald et al. (2003) (Fig. 1), are given as:

$$\begin{aligned}
\chi_D &= -0.022,\\
\chi_{f,1} &= -4.78\times10^{-5}\left(\mathrm{K}^{-1}\right),\\
\chi_{f,2} &= +6.75\times10^{-9}\left(\mathrm{K}^{-2}\right),\\
\chi_{G,1} &= +14.834\times10^{-5}\left(\mathrm{K}^{-1}\right),\\
\chi_{G,2} &= -1.6025\times10^{-7}\left(\mathrm{K}^{-2}\right),\\
\chi_{G,3} &= +6.9907\times10^{-11}\left(\mathrm{K}^{-3}\right), \text{ and}\\
\chi_{G,4} &= -1.1142\times10^{-14}\left(\mathrm{K}^{-4}\right).
\end{aligned} \tag{13}$$

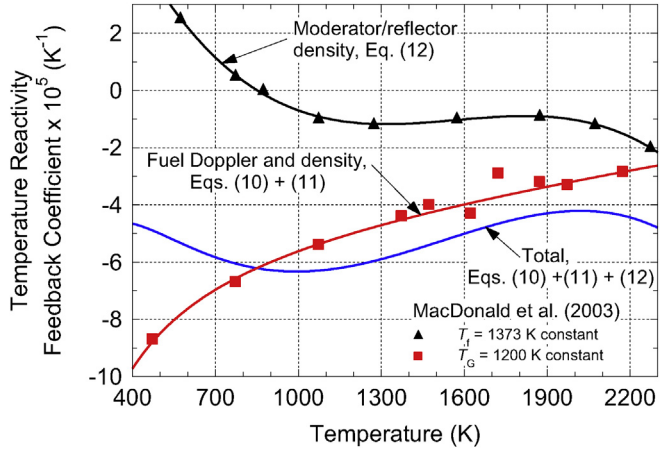

Fig. 1. Reported results (MacDonald et al., 2003) and Least Square Fits of the Temperature Reactivity Feedbacks for the NGNP Reactor.

The small scatter in the calculated results in Fig. 1 had been attributed to a mismatch in the uranium and graphite temperature neutron cross-section libraries, and the differences in the MCNP uranium (both ^{235}U and ^{238}U) cross-section libraries (MacDonald et al., 2003). Below 927 °C, neutron cross-sections were generated using ENDF/B/VI Revision 2 data, and using the ENDF/B/VI Revision 5 data above 1000 °C.

The fuel and graphite temperatures, T_f^o and T_G^o in Equations (10)–(12), are the volume-averaged values in the reactor, at initial steady-state condition, when $\rho_D = \rho_f = \rho_G = 0$ and $\rho = \rho_{ext} = \rho_o$ (Equation (8)). These volume-averaged temperatures are calculated during the initialization phase, prior to simulating a transient, using a thermal model of the prismatic NGNP reactor, described later in this paper. These temperatures are supplied to the PK model. Equations (10)–(12) ensure that initially, at $t = 0$, the calculated reactivity feedbacks are nil ($\rho_D = \rho_f = \rho_G = 0$), and that equilibrium conditions, Equation (6)–(8), are satisfied.

1.3. Delayed-neutron group data

The delayed-neutron groups data in MELCOR-H_2 are those obtained from comprehensive measurements carried out at the Los Alamos National Laboratory using the bare metal assembly, Godiva (Keepin, 1965, Section 4.1). These measurements are of the delayed neutrons from the fast fission of 6 nuclides, U^{235}, U^{233}, U^{238}, Pu^{239}, Pu^{240} and Th^{232}, and from the thermal fission of 3 nuclides, U^{235}, U^{233} and Pu^{239}. For the prismatic NGNP, helium-cooled and graphite moderated thermal reactor, the data of the delayed neutrons from the thermal fission of U^{235} are used.

This data, listed in Table 1, is taken from Table 4.8 of Keepin (1965). The total absolute delayed-neutron yield is 0.0158 (Keepin, 1965, Tables 4.8 and 4.12). This is the total number of delayed-neutrons produced per fission. Since the average number of neutrons produced per thermal fission in U^{235} is $\nu = 2.432$ (Keepin, 1965, Table 4.14), then $\overline{\beta} = 0.0158/2.432 = 0.0065$. The effective fractions of the individual delayed neutron precursors are then calculated as: $\beta_i = \overline{\beta} \times f_i$.

1.4. Numerical solution

The fundamental difficulty in devising a stable and accurate numerical solution of the six-group point kinetics equations is the stiff exponential nature of the solution. A close examination of Equations (1) and (2) reveals the existence of seven different time scales of the exponential solution: $\{1/\lambda_i\}$, $i = 1$ to 6, and $\Lambda/(\rho - \overline{\beta})$. While the shortest time scale of the decay processes, $1/\lambda_6 \approx 1/3$ s is relatively large, the neutron generation time scale is several orders of magnitude smaller. In a fast-spectrum nuclear reactor, the neutron generation time, $\Lambda = (\nu\nu\Sigma_f)^{-1}$, ranges from 50 μs to 1.0 ms, while in a thermal-spectrum reactor, Λ, is much larger in magnitude, ~10 ms. Owing to these very short time scales, conventional explicit integration methods, such as Euler's and higher-order Runge-Kutta (Gill, 1951) require a highly restrictive (short) time

Table 1
Delayed-Neutron data for Thermal Fission of U-235 in NGNP Reactor (MacDonald et al., 2003).

Group index, i	Half-life, $\tau_{1/2}$, (s)	Decay constant, λ_i, (1/s)	Relative abundance, f_i	Absolute group yield (%)
1	55.72	0.0124	0.033	0.052
2	22.72	0.0305	0.219	0.346
3	6.22	0.111	0.196	0.310
4	2.30	0.301	0.395	0.624
5	0.610	1.14	0.115	0.182
6	0.230	3.01	0.042	0.066
Sum	–	–	1.000	1.580

steps to avoid exponential amplification of the error, with unreasonably large computation time for convergence (Greenspan et al., 1968).

Higher-order corrections to the Prompt Jump Approximation (PJA) have been proposed in the literature, such as those of Goldstein and Shotkin (1969), to predict the transient behavior of fast-spectrum reactors. However, the accuracy of the solution decreases with increasing the neutron generation lifetime, Λ. Therefore, the PJA is not suitable for predicting the transient behavior of thermal-spectrum reactors. Besides, the full six-group point kinetics equations need to be solved simultaneously.

The technique developed herein for solving the 6-point kinetics equations (1) and (2) capitalizes on the work of Porsching (1966). These equations, recast in a vectorial form using the similarity variables:$P = \Psi_1$, $Y_i = \Psi_{i+1}$, where $i = 1$ to 6, become:

$$\frac{d\,\Psi_1}{dt} = \frac{\rho - \overline{\beta}}{\Lambda} \times \Psi_1 + \sum_{i=1}^{6} \lambda_i \Psi_{i+1} + S_o \tag{14}$$

$$\frac{d\,\Psi_{i+1}}{dt} = \frac{\beta_i}{\Lambda} \times \Psi_1 - \lambda_i \Psi_{i+1}, \text{ where, } i = 1 \text{ to } 6 \tag{15}$$

Equations (14) and (15) may be written in matricial form as follows:

$$\frac{d}{dt}[\Psi] = \{A\}\cdot[\Psi] + [S], \text{ with } [\Psi] = [\Psi_o] \text{ at } t = 0. \tag{16}$$

The vectors $[\Psi]$ and $[S]$ are given by $[\Psi] = [\Psi_1 \quad \Psi_2 \quad \Psi_3 \quad \Psi_4 \quad \Psi_5 \quad \Psi_6 \quad \Psi_7]^T$ and $[S] = [S_o \quad 0 \quad 0 \quad 0 \quad 0 \quad 0 \quad 0]^T$, respectively, and the 7×7 matrix {A} has the form:

$$\{A\} = \begin{bmatrix} A_{11} & \ldots\ldots & A_{17} \\ A_{21} & \ldots\ldots & A_{27} \\ \ldots. & \ldots\ldots & \ldots. \\ \ldots. & \ldots\ldots & \ldots. \\ A_{71} & \ldots\ldots & A_{77} \end{bmatrix} = \begin{bmatrix} \left(\rho - \overline{\beta}\right)/\Lambda & \lambda_1 & \lambda_2 & \ldots\ldots & \lambda_6 \\ \beta_1/\Lambda & -\lambda_1 & 0 & \ldots\ldots & 0 \\ \beta_2/\Lambda & 0 & -\lambda_2 & \ldots\ldots & 0 \\ \ldots\ldots\ldots & \ldots\ldots & \ldots\ldots & \ldots\ldots & \ldots\ldots \\ \beta_6/\Lambda & 0 & 0 & \ldots\ldots & -\lambda_6 \end{bmatrix}. \tag{17}$$

Note that the coefficient A_{11} is the only time-dependent coefficient in the {A} matrix, through control actions of the reactor and Doppler and temperature reactivity feedbacks.

1.4.1. Special case: constant total reactivity and neutron source term

For constant and time independent total reactivity, ρ, and neutron active source termS_o, a solution of the homogeneous equation (with $[S] = 0$) is:$\{\exp(At)\}\cdot[\Phi]$, where $[\Phi]$ is an arbitrary constant vector. For an arbitrary matrix {M}, the power series $\{\Im\} + \{M\} + \{M\}^2/2! + \{M\}^3/3! + \ldots$ converges to a matrix called the exponential {M}, which is denoted {exp(M)}. An obvious particular solution of Equation (16) is the constant vector (independent of time): $(-\{A\}^{-1}\cdot[S])$. Therefore, the solution of Equation (16) can be written as:

$$[\Psi] = \{\exp(At)\}\cdot[\Phi] - \{A\}^{-1}\cdot[S]. \tag{18}$$

The unknown vector $[\Phi]$ is obtained from satisfying the initial condition (Equation (7)), as:

$$[\Psi_o] = \{\Im\}\cdot[\Phi] - \{A\}^{-1}\cdot[S]. \tag{19}$$

In this equation, $\{\Im\}$ is the Identity matrix; which results in:

$$[\Phi] = [\Psi_o] + \{A\}^{-1}\cdot[S]. \tag{20}$$

Finally, the exact solution of Equation (16), for constant reactivity and source term, takes the form:

$$[\Psi] = \{\exp(At)\}\cdot\left([\Psi_o] + \{A\}^{-1}\cdot[S]\right) - \{A\}^{-1}\cdot[S]. \tag{21}$$

Equation (21) suggests the following algorithm for advancing the numerical solution in time (Porsching, 1966). Assuming the solution $[\Psi]_n$ is known at time t_n, the solution at time $(t_{n+1} = t_n + \Delta t)$ takes the form:

$$[\Psi]_{n+1} = \{\exp(A\,\Delta t)\}\cdot\left([\Psi]_n + \{A\}^{-1}\cdot[S]\right) - \{A\}^{-1}\cdot[S]. \tag{22}$$

In practice, since the total reactivity and active source term change over the interval $[t_n, t_{n+1}]$, the following "average" values of the coefficients A_{11} and S_o are used during this time step:

$$A_{11} = \frac{\theta\rho_{n+1} + (1-\theta)\rho_n - \overline{\beta}}{\Lambda}, \text{ and} \tag{23a}$$

$$S_o = \theta(S_o)_{n+1} + (1-\theta)(S_o)_n, \tag{23b}$$

where $0 < \theta < 1$. A $\theta = 0.5$, provides the best accuracy in time. Porsching (1966) has shown that the local discretization error of the method defined by Equation (22) is third-order accurate in time $(\Delta t)^3$. The advantages of this method are preserving the original form of the point kinetics equations, and capturing the exponential behavior of the solution, using a suitable approximation to the exponential matrix $\exp\{A \times \Delta t\}$.

1.4.2. Approximation of exponential matrix

Any method based on the truncation of the exponential power series would yield highly inaccurate results, unless the time step is severely restricted. With an incredibly small time step, the power series defining the exponential converges too slowly for practical use. For example, using the first 2 terms of the series$\exp\{M\} \approx \{\Im\} + \{M\}$, is equivalent to using the Euler's

approximation to solve the PK equations. Similarly, the simplified Runge-Kutta is equivalent to approximating the exponential matrix using the first 3 terms of the series:$\exp\{M\} \approx \{\Im\} + \{M\} + \{M\}^2/2$. When applied to the solution of the point kinetics equations, both of these methods require unreasonably small time steps to avoid exponential growth of the error and to ensure stability of the solution (Porsching, 1966; Greenspan et al., 1968). To avoid these shortcomings, Porsching (1966) has suggested using rational matrix functions to approximate the exponential matrix for solving the point kinetics equations. He proposed different approximations of different accuracies (Table 2).

1.5. Padé approximants of the exponential matrix

The Padé(p,q) rational function or "approximant" is the ratio of two polynomials, of degrees p in the numerator and q in the denominator (Baker, 1975; Ward, 1977; Van Loan, 1977). It approximates a particular function F(x) to an order $O(x^{p+q+1})$. The coefficients of the polynomials are obtained from the coefficients of the Taylor series expansion of the function. An advantage of the Padé approximants is providing bounded and stable values over a much wider domain than a conventional Taylor series approximation, which diverges quickly away from the chosen expansion point. The Padé approximant's power series generally agrees with the power series of the function it is approximating.

Some of the ground work on the Padé approximants had been established early in the 19th century by Forbenius (1881). Padé (1892), apparently unaware of previous work, was the first to emphasize the importance of displaying the functions in tabular form, and studying the structure of the table (Baker, 1975). Different Padé approximants to the exponential function $\exp(x)$ are listed in Table 2 (Baker, 1975). A few of these approximants are compared in Fig. 2 to the exponential function. The results in this figure indicate the range where a Padé approximant is an accurate representation of the function $\exp(x)$, which increases with increasing values of $(p + q)$.

Various Padé approximants of the exponential matrix, i.e.

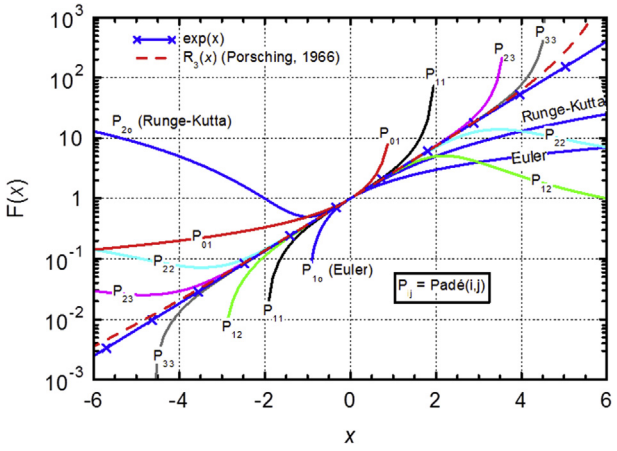

Fig. 2. Comparison of Padé Approximants of the Exponential Function, exp(x).

Padé(0,1), (1,2), (2,2) and (3,3), are investigated in this work, and the Padé(3,3) function is chosen for the higher accuracy and wide range of applicability (Fig. 2).

To evaluate the accuracy of the numerical solution, the present results are compared to those of the Inhour analytical solution for a step reactivity insertion. The delayed-neutron group data, such as the decay constants and yields, are those for the thermal fission of ^{235}U (Table 1). The neutron generation time, $\Lambda = 10^{-2}$s, is representative of that for a graphite-moderated, thermal spectrum reactor. To examine the stability and accuracy of the proposed numerical technique, a constant prompt critical reactivity insertion of \$1.0 is applied, increasing the reactor thermal power by an order of magnitude in 8s, two orders of magnitude in 16s, and four orders of magnitude in only 32s. Results for this test case (step external reactivity insertion of $\rho/\overline{\beta} =$ \$1.0, with no active neutron source, $S_o = 0$, and $\Lambda = 10^{-2}$ s) are shown in Fig. 3.

When using a fixed time step, $\Delta t = 4$s, after 40s into the transient (at which the reactor thermal power increases by a

Table 2
Padé(p,q) Approximants to the Exponential Function, $\exp(x)$ (Baker, 1975).

p	$q = 0$	$q = 1$	$q = 2$	$q = 3$
0	$\frac{1}{1}$	$\frac{1}{1-x}$	$\frac{2}{2-2x+x^2}$	$\frac{6}{6-6x+3x^2-x^3}$
1	$\frac{1+x}{1}$	$\frac{2+x}{2-x}$	$\frac{6+2x}{6-4x+x^2}$	$\frac{24+6x}{24-18x+6x^2-x^3}$
2	$\frac{2+2x+x^2}{2}$	$\frac{6+4x+x^2}{6-2x}$	$\frac{12+6x+x^2}{12-6x+x^2}$	$\frac{60+24x+3x^2}{60-36x+9x^2-x^3}$
3	$\frac{6+6x+3x^2+x^3}{6}$	$\frac{24+18x+16x^2+x^3}{24-6x}$	$\frac{60+36x+9x^2+x^3}{60-24x+3x^2}$	$\frac{120+60x+12x^2+x^3}{120-60x+12x^2-x^3}$

Euler

Standard Runge-Kutta

Present Numerical technique

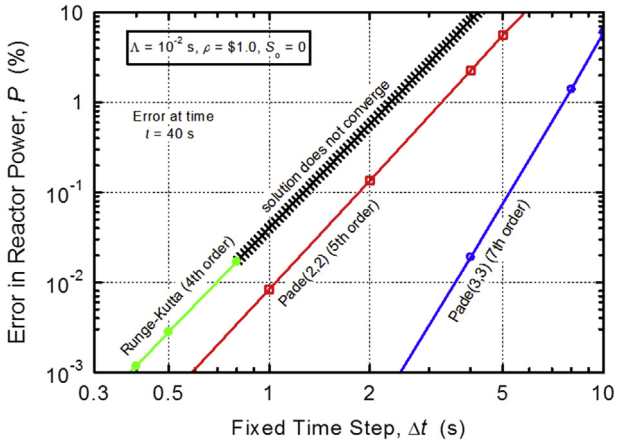

Fig. 3. Effect of Time Step Size on the Accuracy and Stability of Numerical Solution of Point Kinetics Equations, for $1.0 step Reactivity Insertion, using Different Padé Approximants and the Runge-Kutta (4th order) Approximation.

integration technique (Gill, 1951), do not converge for time steps > 0.8s. Conversely, the present exponential matrix method with the Padé(3,3) approximant, is 7th order accurate and could use a time step that is an order of magnitude larger than that of the 4th-order Runge-Kutta technique, for the same discretization error (Fig. 3).

Table 3 compare the effect of the calculation time step (4s and 8s) on the error in the calculated fission power of the present solution using the Padé(3,3) approximant, compared the Inhour analytical solution for a step reactivity insertion of $1.0. As indicated in this table, the error of the present solution with 4s time step size in negligibly small (0.004–0.019%), depending on the duration of the transient). It increases with doubling the calculation time step to 8s, but still small (~0.3–1.4%).

The accuracy of the present solution of the PK equations is further investigated for the reactivity insertion cases (a) - (c) in Fig. 4. The results are presented in Fig. 5. These results further confirm the accuracy and robustness of the present solution of the six-group point kinetics equations (1) and (2). Thus, the Padé(3,3)

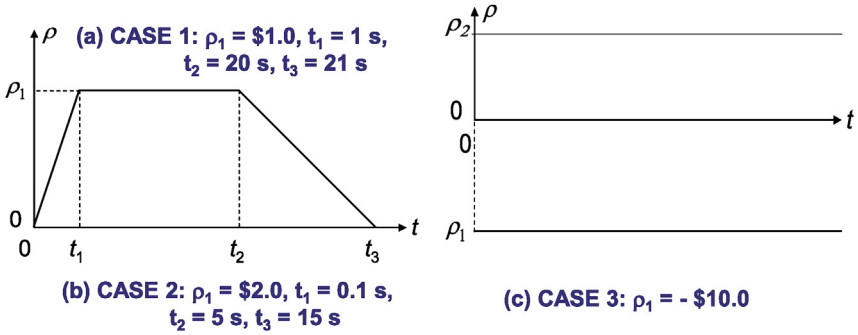

Fig. 4. Cases examined for the accuracy of the present solution using the Padé(3,3) approximant.

factor ~ 10^5), the error in the thermal power using the Padé(1,2), Padé(2,2) and Padé(3,3) approximant is 28%, 2.3% and 0.019%, respectively. The Padé(1,2) approximant is accurate to the order $O(x^4)$, while Padé(2,2) is accurate to the order $O(x^5)$, and Padé(3,3) to the order $O(x^7)$. Regarding the computation time for solution convergence, the exponential matrix numerical techniques with the Padé approximants are nearly identically, since they all require solving two 7×7 linear systems of equations by Gauss elimination at each time step and/or internal iteration to resolve the change in the total reactivity due to the feedback effects. In the absence of an active neutron source, only a single Gauss elimination is required per time step.

The error of the present approximate numerical solution using the Padé approximants increases with increased time step size (Fig. 3). With a relatively large time step, Δt, of 2s, the error is less than 0.001% after $t = 40$s, corresponding to a 10^5 increase in the reactor thermal power. This calculation required only 20 time steps for convergence. Doubling the time step size to 4s increases the error to 0.02% after 40s into the transient. Even with an unreasonably large time step of 8s, during which the reactor thermal power increases tenfold, the local discretization error at each time step is only ~0.3%. Such very low discretization errors demonstrate the ability of the Padé(3,3) approximant to accurately capture the exponential behavior of the solution of the point kinetics equations. Owing to the robustness, good stability and accuracy of the present numerical solution with the Padé(3,3) approximant, higher order approximants are not considered.

The results in Fig. 3, using the 4th order Runge-Kutta numerical exponential matrix numerical technique is suitable for all practical reactor transients of interest. Furthermore, when the point kinetics equations are coupled to the thermal-hydraulics model of the reactor, through various temperature reactivity feedbacks, the maximum time step of the present numerical technique is unrestricted. This technique with the Padé(3,3) approximant is stable and accurate even for more than a ten-fold increase in the reactor thermal power per time step. Such attribute make the present solution of the point kinetics equations suitable for incorporation into large reactor safety analysis codes such as RELAP5-3D and MELCOR-H2 (Rodriguez et al., 2007; RELAP5-3D© Code Development RELAP5-3D Code Development Team, 2012).

Table 3
Effect of Time Step size, Δt, on the Accuracy of the Present Solution using the Padé(3,3) approximant of the fission power following a $1.0 step reactivity Insertion.

Transient time (s)	Inhoursolution	Padé(3,3), Δt = 4 s		Padé(3,3), Δt = 8 s	
	(P/P_o)	(P/P_o)	Error (%)	(P/P_o)	Error (%)
0	1	1		1	–
4	4.64036	4.64113	0.017	–	–
8	14.5063	14.5069	0.004	14.5517	0.313
12	43.5872	43.5897	0.006	–	–
16	129.913	129.923	0.008	130.636	0.557
20	386.426	386.463	0.010	–	–
24	1148.79	1148.93	0.012	1158.39	0.836
28	3414.7	3415.15	0.013	–	–
32	10149.5	10151	0.015	10262.6	1.114
36	30166.7	30171.9	0.017	–	–
40	89662.8	89679.7	0.019	90913.9	1.395

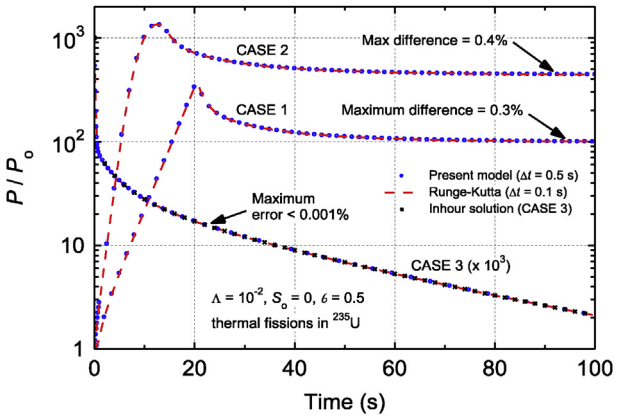

Fig. 5. Accuracy of the Present solution of the Kinetics Equations for External Reactivity Insertion Cases in Fig. 4.

1.5.1. Solution implementation

The present numerical solution of the 6-group point kinetics equations using the Padé(3,3) approximant of the exponential matrix, is implemented as follows:

(a) Once the coefficients A_{11} and S_o have been updated using Equation (23), the solution uses Gauss elimination with partial pivoting and row normalization (Golub and van Loan, 1984) to compute the vector of dimension 7:

$$[\mathrm{B}] = \{A\}^{-1} \cdot [\mathrm{S}] \tag{24}$$

(b) The solution then calculates the vector [C] and the 7 × 7 matrix {X}:

$$[\mathrm{C}] = [\Psi]_n + [\mathrm{B}], \text{ and } \{X\} = \{A\} \times \Delta t. \tag{25}$$

(c) Subsequently, the exponential matrix is approximated using the Padé(3,3) rational function (Table 2), as:

$$\{\exp(X)\} \cong \left\{\Im - \frac{X}{2} + \frac{X^2}{10} - \frac{X^3}{120}\right\}^{-1} \cdot \left\{\Im + \frac{X}{2} + \frac{X^2}{10} + \frac{X^3}{120}\right\}. \tag{26}$$

Equation (22) becomes:

$$[\Psi]_{n+1} = \left\{\Im - \frac{X}{2} + \frac{X^2}{10} - \frac{X^3}{120}\right\}^{-1} \cdot \left\{\Im + \frac{X}{2} + \frac{X^2}{10} + \frac{X^3}{120}\right\} \cdot [\mathrm{C}] - [\mathrm{B}]. \tag{27}$$

(d) This linear system of equations is easily solved by computing the vector:

$$[\mathrm{E}] = \left\{\Im + \frac{X}{2} + \frac{X^2}{10} + \frac{X^3}{120}\right\} \cdot [\mathrm{C}]. \tag{28}$$

The (7 × 7) linear system for the vector [D] is then calculated using Gauss elimination with partial pivoting and row normalization, as:

$$[\mathrm{D}] = \left\{\Im - \frac{X}{2} + \frac{X^2}{10} - \frac{X^3}{120}\right\}^{-1} \cdot [\mathrm{E}] \tag{29}$$

Subsequently, the solution vector is advanced in time as:

$$[\Psi]_{n+1} = [\mathrm{D}] - [\mathrm{B}]. \tag{30}$$

1.6. Application to transient operation of NGNP reactor

This section presents dynamic simulation results of the prismatic NGNP reactor, by coupling the present point kinetics model to 84-nodes thermal-hydraulics model of the reactor (Matlab, 2004; Simulink, 2004; Shampine and Reichelt, 1997; Shampine et al., 1999). Fig. 6 shows a radial cross-sectional view and Fig. 7 presents an axial cross-section view of the NGNP reactor. The annular core, comprised on three concentric rings of prismatic fuel elements, 80 cm-high with a flat-to-flat of 36.2 cm, is surrounded by hexagonal graphite elements of the inner and outer reflector. The 102 fuel elements of the core stacked in columns, 10 elements tall, occupy ring 6, 7 and 8 (Figs. 4 and 5). The core fuel elements have a total of 10,626 vertical channels, 16 mm in diameter, for the flow of the helium coolant through the annular core, and a total of 20,700 vertical cavities (12.7 mm in diameter) loaded with TRISO particle fuel compacts, 12.5 mm in diameter. The total mass of the graphite moderator in the fuel elements of the driver core is ~97.8 metric tons (~19.63% of the total graphite mass in the reactor core).

The 61 assemblies of the inner graphite reflector in the NGNP reactor core occupy the 5 innermost rings and weigh ~99 metric tons (~19.87% of the total graphite mass in the reactor core). The 131 graphite elements of the outer reflector occupy the 3 outermost rings of the core, extending its outer diameter to 6.54 m. They weigh 212.4 metric tons (~42.63% of total graphite mass in the reactor core) (Fig. 7). More details on the design of NGNP reactor and components can be found elsewhere (IAEA, 2001; MacDonald et al., 2003, 2004, Travis and El-Genk, 2013).

The graphite elements of the upper (level 12) and lower (level 1) axial reflectors, above and below the core elements (levels 2 to 11) (Fig. 5), weigh 44.5 metric tons each (~17.86% of total graphite mass in the reactor core). The calculated masses of the graphite in the reactor core and both the axial and radial reflectors for the reported reactor geometry (MacDonald et al., 2003, 2004), assume a nuclear graphite density of 1.778 kg/m^3 (an average volume porosity of 0.21).

The helium gas coolant enters the reactor pressure vessel at the bottom, and flows upward through 6 pairs of annular channels on the outside of the core barrel, for cooling the reactor pressure vessel wall (Figs. 6 and 7). In the upper plenum, the helium gas reverses direction and flows downward through 10,626 coolant channels in the top graphite axial reflector and the annular core fuel elements. The hot helium exiting the core flows through the bottom graphite axial reflector into the lower plenum, where it mixes before exiting the reactor pressure vessel to the turbomachinery for energy conversion (MacDonald et al., 2003, 2004; Rodriguez and El-Genk, 2010; Travis and El-Genk, 2013).

1.6.1. NGNP reactor thermal hydraulic model

The developed nodal average thermal hydraulics model of the NGNP reactor divides the core, including the top and bottom axial graphite reflector, into 12 axial regions, each comprised of 7 concentric radial zones, for a total of 12 × 7 = 84 temperature nodes. The energy conservation in each zone and the thermal conductance between zones are expressed in terms the nodal

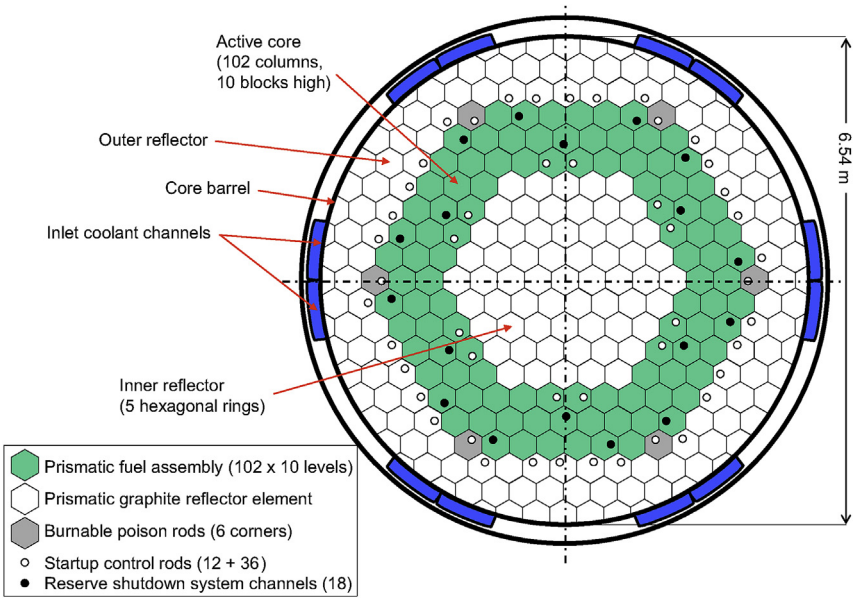

Fig. 6. Radial cross-section of NGNP reactor core (MacDonald et al., 2003, 2004).

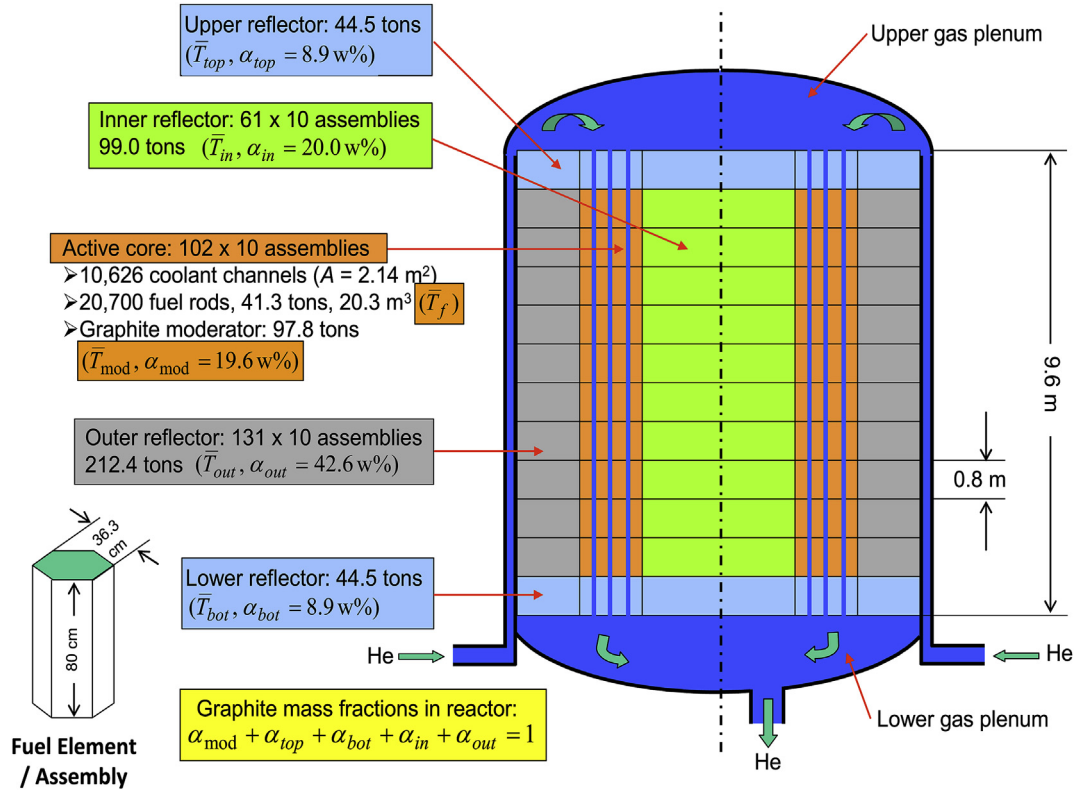

Fig. 7. An Elevation View of the Prismatic core, NGNP Reactor (MacDonald et al., 2003, 2004) in the Developed Thermal-Hydraulics Model.

temperatures, which are basically the volume-averaged values at steady-state condition. The calculated average temperatures in the seven radial zones in each axial region (0.8 m tall each) are of: (a) the TRISO fuel compact rods, $\overline{T}_f$ (or graphite plugs in the top and bottom axial graphite reflector, $\overline{T}_{top}$ and $\overline{T}_{bot}$); (b) the graphite moderator in the core fuel elements, $\overline{T}_{\text{mod}}$; (c) the helium gas flow in the circular channels in the vertical columns of the stacked fuel elements in the active core, $\overline{T}_{co}$; (d) the inner graphite reflector, $\overline{T}_{in}$; (e) the outer radial graphite reflector; $\overline{T}_{out}$ (f) the metal reactor vessel wall; $\overline{T}_w$ and (g) the helium gas flowing in the vertical annuli between the core barrel and the reactor vessel wall (Fig. 7). The developed thermal-hydraulics model accounts for the thermal energy storage capacities of the different zones, the axial and radial conduction between zones, the convective heat transfer between the solid structures and helium coolant (Travis and El-Genk, 2013), and the radiative heat transfer through the transparent helium gas

in the upper and lower plenums of the reactor vessel.

The reactor thermal-hydraulics and point kinetics models are coupled through the temperature reactivity feedbacks (Equations (9)–(12) and Fig. 1). The thermal hydraulics model calculates the volume-averaged temperatures of the fuel compact ($\overline{T}_f$) in the annular core, the inner graphite reflector ($\overline{T}_{in}$), the graphite moderator in the core fuel elements ($\overline{T}_{\rm mod}$), and the graphite radial outer reflector ($\overline{T}_{out}$), using a simple weighed average of the seven radial nodal temperatures associated with each the 10 axial regions of the reactor core (Fig. 7). The volume-averaged temperatures of the upper ($\overline{T}_{top}$) and lower ($\overline{T}_{bot}$) graphite axial reflector are calculated by averaging the nodal temperatures in the axial regions 12 and 1, respectively. The mass-averaged (or volume-averaged) temperature of the graphite in the reactor core$\overline{T}_G$, for determining the moderator temperature reactivity feedback, Equation (12), is calculated based on the graphite mass fractions, α_i, in the various regions of the core (Fig. 7), as:

$$\overline{T}_G = \alpha_{in}\overline{T}_{in} + \alpha_{\rm mod}\overline{T}_{\rm mod} + \alpha_{out}\overline{T}_{out} + \alpha_{top}\overline{T}_{top} + \alpha_{bot}\overline{T}_{bot}, \quad (31)$$

where,

$$\alpha_{in} + \alpha_{\rm mod} + \alpha_{out} + \alpha_{top} + \alpha_{bot} = 1. \quad (32)$$

The calculated volume averaged temperatures of the fuel compacts, $\overline{T}_f$, and the reactor graphite, $\overline{T}_G$, are substituted into Equations (10)–(12), for calculating the various temperature reactivity feedbacks for the point kinetics model.

1.7. Simulation results of NGNP reactor transients

The coupled point kinetics and thermal-hydraulics models of the NGNP reactor account for the fuel and graphite moderator/reflector temperature reactivity feedbacks and Doppler Broadening. The coupled models are used in this section simulate the transient response of the NGNP reactor during a startup and following an external reactivity insertion. The calculated reactor parameters include the total reactivity and the reactor thermal power, the average fuel and graphite temperatures, and the helium coolant temperature, as functions of time during the simulated transients.

1.7.1. Simulated negative reactivity insertion transient

To demonstrate the capability of the present PK model, dynamic simulation of the NGNP reactor is performed following gradually external reactivity insertion (Fig. 8). Initially, at time zero, the steady-state operating reactor has been at a nominal thermal power of 600 MW_{th} ($S_o = 0$, $\rho_o = 0$) for 100s, followed by a gradual insertion of negative external reactivity of \$0.5, at a constant rate over a period of 300s. The negative external reactivity insertion is held steady for 600s then followed by a gradual insertion of a positive external reactivity of the same amount (\$0.5) and at the same rate, over a period of 300s. Thus, the total dynamic simulation time is 1,200s (20 min) (Fig. 8).

Fig. 8 presents the profile of external reactivity insertion used in the simulated transient of the NGNP reactor. The thermal-hydraulics model of the NGNP reactor calculates initial steady-state average fuel and graphite temperatures of $T_f^o = 1160$ K and $T_G^o = 1127.4$ K, respectively. These values are in good agreement with those reported by MacDonald et al. (2003), 1164 K and 1114 K, respectively, for the same reactor thermal power, and helium coolant mass flow rate of 226.6 kg/s and inlet temperature of 763 K, used in the simulated transient. During this transient, initiated at 100s (Fig. 8), the helium coolant inlet temperature and mass flow rate through the reactor core are kept constant, but the helium coolant exit and average temperatures are calculated and change during the simulated transient, commensurate with the changes in reactor thermal power. The results of the simulated transient are delineated in Figs. 9–11.

When the external reactivity insertion stops and is kept steady at \$0.5, 300s from the start of the simulated transient, the reactor thermal power is lowest at ~472 MW_{th}. The total reactivity of a negative ~ ¢0.95 increases to a positive ¢1.6, causing the reactor thermal power to peak at 510 MW_{th}, before dropping approaching a steady value of ~498 MW_{th}, ~420s from the start of the simulated transient. Note that, at steady state operation of the NGNP at 600 MW_{th}, the average fuel temperature (~1160 K) is higher than that of the graphite in the core (~1128 K) (Figs. 10 and 11). Conversely, at ~200s from the start of the simulated transient, the average fuel temperature drops below that of the graphite (Fig. 11), approaching a steady value (~1100 K) that is lower than that for the graphite (1113 K). This is because of the faster release of the energy stored in the fuel particles when the reactor thermal power is decreasing (Fig. 11).

The external reactivity insertion of a negative \$0.5 is kept steady for 600s, 300s–900s from the start of the simulated transient, then increased at a steady rate of ¢1.67/s, to zero, 1200s after the start of the transient (Fig. 8). The total reactivity increases rapidity, peaks at a positive ¢2.2, then drops to a positive ¢0.8, when the external reactivity insertion ceases, 1200s from the start of the simulated

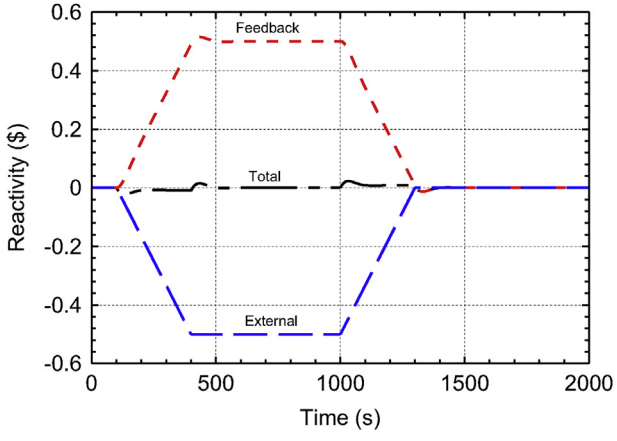

Fig. 8. Changes in external reactivity insertion and total reactivity and temperature reactivity feedback during the simulated operation transient of the NGNP reactor.

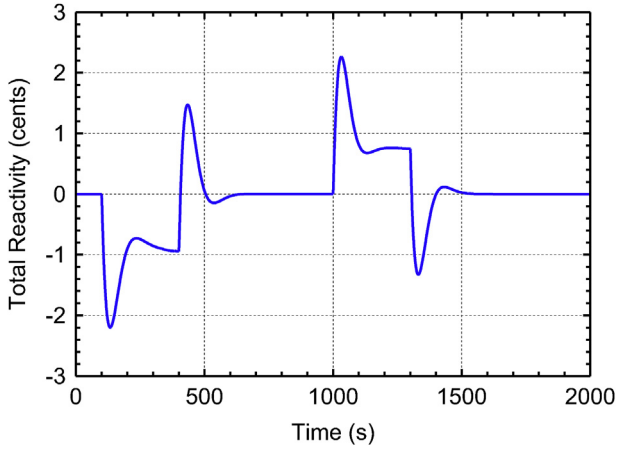

Fig. 9. Calculated changes in the total reactivity during simulated transient of NGNP.

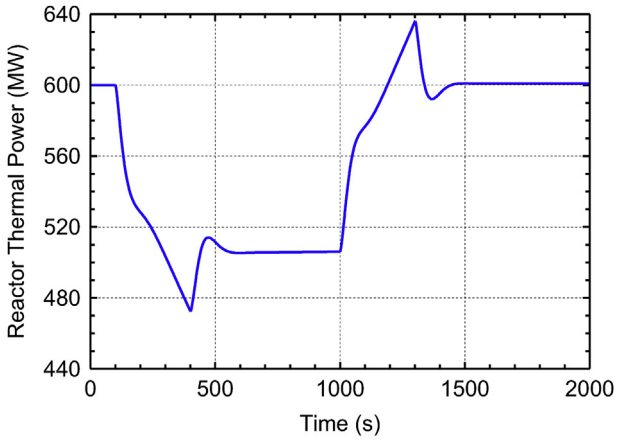

Fig. 10. Calculated changes in thermal power of NGNP reactor in the simulated transient.

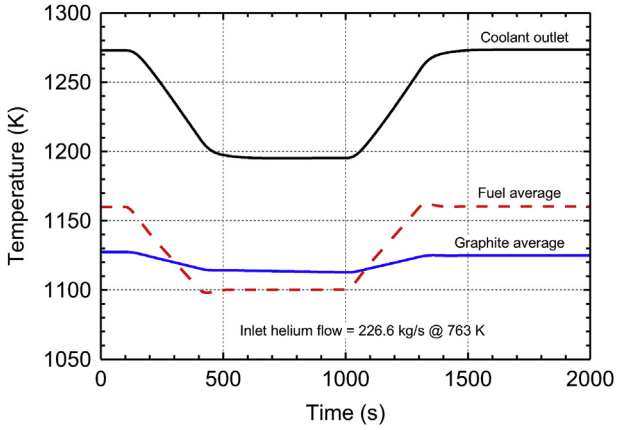

Fig. 11. Calculated changes in average fuel and graphite temperatures during simulated transient of the NGNP reactor.

transient (Figs. 8 and 9). At such time, the reactor thermal increases rapidly to a peak of ~636 MW_{th}, causing the average fuel and graphite temperatures to increase, and approach steady values of ~1160 K, and 1125 K, respectively. Such temperatures introduce a negative reactivity feedback, causing the total reactivity of the NGNP reactor to drop to a minimum of a negative ¢1.3, before recovering rapidly approaching zero, for steady state operation, ~1400s from the start of the simulated transient (Fig. 9). At such time, the reactor thermal power, the temperature of helium coolant exiting the reactor core and both the fuel and graphite average temperatures are the same as those during steady state operation of the NGNP reactor before the start of the simulated transient (Figs. 10 and 11). The simulated transient in Figs. 8–11, used a fixed time step size, Δt, of 1 s and an implicit/explicit discretization parameter, $\theta = 0.50$ (Equation (23a) and (23b)). The solution of the coupled thermal-hydraulics and point kinetics models of the NGNP reactor was fast to run on a modest work station.

The solution of the coupled models used an adaptive step size, based on the methodology proposed by Keepin and Cox (1960). Because the peaks of the reactor thermal power and temperatures during the simulated transients do not occur at the same time (Figs. 10 and 11), a dimensionless parameter, δ, is introduced to evaluate the suitability of the time step size, depending on the relative transient changes in the reactor thermal power and the fuel average temperature. This parameter is expressed as:

$$\delta = \mathrm{DMAX1}\left(\frac{|P_{n+1} - P_n|}{P_n} \;,\; 10 \times \frac{\left|\left(\overline{T}_f\right)_{n+1} - \left(\overline{T}_f\right)_n\right|}{\left(\overline{T}_f\right)_n} \right), \qquad (33)$$

In this equation, the subscript n refers to the calculated values at the old (previous) time step, and the subscript $(n+1)$ refers to the values calculated at the current time step. The dimensionless parameter, δ, is an indicator for the need to change the time step size, Δt, in the simulated transient After obtaining the solution of the coupled thermal-hydraulics and point-kinetics models of the NGNP reactor in the previous time step size, the performed tests to assess the need to change the time step or keep it unchanged in subsequent calculations, are as follows:

(a) If $\delta < F_1$, the time step size is increased by a factor $\gamma > 1$;
(b) If $F_1 \le \delta < F_2$, the solution is advanced in time with the time step unchanged; *this is the preferred change for the reactor thermal power and temperatures*;
(c) If $F_2 \le \delta$, the time step size is decreased by the factor $\gamma > 1$.

A factor $\gamma = 1.2$ provides good results. In addition to these criteria, the solution of the coupled point kinetics and thermal-hydraulics models of the NGNP reactor during the simulated transients, imposes minimum and maximum values of the time step size, not be exceed.

The simulated reactivity insertion transient of the NGNP reactor, described and discussed earlier, investigated the effect of the following parameters values:

$$\begin{array}{l} \text{(a) } F_1 = 0.05\%,\ F_2 = 0.5\%,\ \text{and } \theta = 0.5; \\ \text{(b) } F_1 = 0.10\%,\ F_2 = 1.0\%,\ \text{and } \theta = 0.5; \\ \text{(c) } F_1 = 0.05\%,\ F_2 = 0.5\%,\ \text{and } \theta = 0.0; \\ \text{(d) } F_1 = 0.10\%,\ F_2 = 1.0\%,\ \text{and } \theta = 0.0. \end{array} \qquad (34)$$

Based the obtained results with an implicit/explicit discretization parameter, $\theta = 0.50$, the maximum error in the calculated reactor thermal power during the 2000s long simulated transient (Figs. 6–9) is 0.1, 0.3, 0.6 and 0.6 MW_{th} for cases (a), (b), (c) and (d) in Equation (34), respectively (the time step size is always > 1 s in all these cases). A fiducial factor F_2 of 0.5% and 1% also gives reasonable accuracy, even with $\theta = 0.0$. With $\theta = 0.0$, the MELCOR-H_2 thermal-hydraulics model of the gas-cooled reactor (Rodrigues et al., 2007) is effectively decoupled from the point kinetics model, requiring no internal iterations to resolve the dependence of the total reactivity on the advanced-time average fuel and graphite temperatures.

At the same time, the external reactivity insertion and the temperature reactivity feedbacks are accounted for explicitly in the point kinetics model (since they are calculated at the previous time step). In MELCOR-H2, the thermal-hydraulics model is coupled to the present point kinetics model, for simulating different transient analyses of VHTRs and HTRs, using the appropriate temperature reactivity feedbacks. Similarly, the present point kinetics model could be applied to other system codes such as RELAP5-3D.

1.7.2. Startup simulation of NGNP reactor

This section presents the results of a startup simulation of the NGNP reactor, initially at a constant temperature of 764 K, a helium inlet flow rate of 226.6 kg/s, a reactor thermal power of 10 W_{th}, initial reactivity of ¢0.193, and an active neutron source power generation rate of 1.254 mW/s (Fig. 12a). The temperature of the helium coolant entering the reactor core is held constant during the simulated startup transient. At 100s, the startup transient begins by an external reactivity insertion at a constant rate for 1900s, during

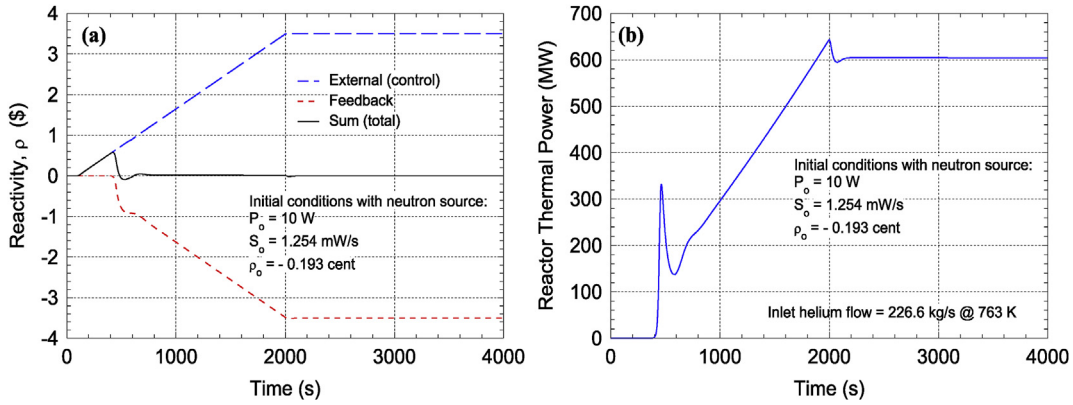

Fig. 12. Calculated total reactivity and thermal power of NGNP reactor during simulated startup transient.

which the total external reactivity is $3.5. Hence thereafter, the external reactivity is held constant (Fig. 12a). At ~400s, the negative reactivity feedback effects stop the increase in the total reactivity, which eventually reach a steady zero value at ~800s of the startup transient. At such time, and thereafter, the values of the positive external reactivity and the negative temperature reactivity feedback are equal in magnitude, maintaining a net zero total reactivity for the NGNP reactor (Fig. 12a).

Fig. 12b presents the calculated transient increase in the reactor thermal power during the simulated startup transient until reaching a steady state value of 600 MW_{th}, at ~2,200s. The increases in the average temperature of the graphite, the helium coolant, the fuel particle, and of the helium gas exiting the reactor core are presented in Fig. 13. The results in this figure show steady temperature increases during the external reactivity insertion phase of the simulated startup transient, and after reaching the steady state values. The values of the steady state temperatures in Fig. 13 are the same as those reported for NGNP reactor (MacDonald et al., 2003, 2004), at same reactor nominal thermal power of 600 MW_{th}, and inlet temperature (763 k) and flow rate (226.6 kg/s) of the helium coolant through the reactor core (Fig. 7).

2. Discussion

The primary objective of this work was to develop a PK model that could be easily coupled to a thermal-hydraulic model of the NGNP reactor in MELCOR-H2 system analysis Code, and which is reasonably accurate and inherently stable with unrestricted time step size. Therefore, the transient simulation of the NGNP would solely subject to the user specified time step for T-H model of the reactor in the system code (typically large time step), and unrestricted by the PK model. This has been demonstrated in this paper.

The development of the PK model and results of the performed analysis in the paper clearly demonstrate the stability and the reasonable accuracy of the applied approximate numerical technique for solving the PK equations in the present model. The focus on the NGNP reactor is a good test case and because the funding for this effort was specifically to develop a PK model to incorporate into MELCOR-H2 for transient analyses of this helium gas cooled nuclear power plant. Nonetheless the developed PK model can be as easily incorporated into system codes for transient analyses of other reactor types such a high temperature reactor (HTR), a sodium fast reactor (SFR), a molten-salt reactor (MSR), and light water reactors (LWRs), given that the appropriate reactivity feedback relations and values, specific to the reactor type and design, are used.

In addition to developing the PK model, a parallel effort included developing a design methodology of Closed Brayton Cycle (CBC) turbomachinery for the NGNP and performing design and performance optimizations (Rodriguez et al., 2007, 2009, El-Genk and Tournier, 2008, 2009, 2010, Tournier and El-Genk, 2009). The CBC turbomachinery model has also been successfully incorporated into MELCOR-H2 (Rodriguez et al., 2007, 2009). Since MELCOR-H2 and RELAP5-3D system codes have similar architecture, the developed PK model could be as easily incorporated into RELAP5-3D, if needed, or in any other system codes developed elsewhere.

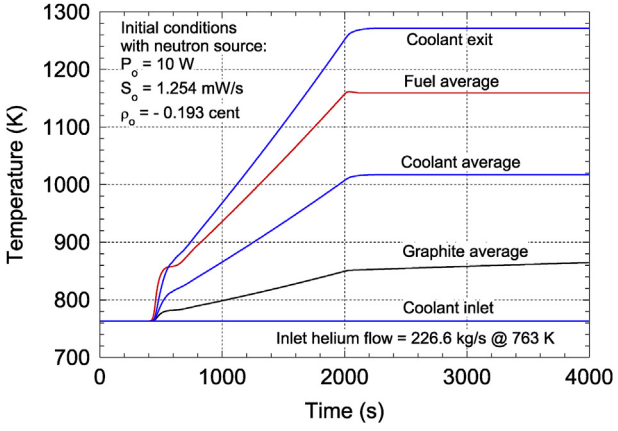

Fig. 13. Calculated Temperatures during the simulated Startup Transient of the NGNP Reactor.

3. Summary and conclusions

This paper developed and demonstrated an accurate, fast-running and stable six-group, point kinetics model for dynamic simulation of the operation of the next generation nuclear plant (NGNP) reactor with unrestrictive time step size. The model solves the coupled nonlinear and stiff six-group point kinetics equations and accounts for Doppler Broadening and the fuel and graphite temperatures reactivity feedbacks. In addition, it includes an active neutron source for zero-power reactor startup and uses an efficient and robust approximation of the exponential matrix using 7th order-accurate Padé(3,3) approximate, with a discretization error on the order of $(\Delta t)^3$.

The developed PK model handles high reactivity insertions, in excess of a prompt critical, $\rho/\bar{\beta}>$ $1.0, with unrestrictive time step size. Results are successfully benchmarked using the Inhour solution for a step insertion of external reactivity. With a 2 s time step,

the error of predicting the reactor thermal power is ~0.001%, increasing exponentially to ~0.08% and ~1.5% with increased time step size to 5 and 8 s, respectively.

To simulate the transient response of the NGNP reactor, following an external reactivity insertion and during a startup, the PK model is coupled to 84-nodes thermal-hydraulics model of the NGNP reactor, also developed in this work. The T-H model divides the reactor core, including the top and bottom axial graphite reflector, into 12 axial regions, each comprised of 7 concentric radial zones, for a total of $12 \times 7 = 84$ temperature nodes. The energy conservation in each zone and the thermal conductance between zones are expressed in terms the volume averaged nodal temperatures. The calculated parameters during the dynamic simulations of the NGNP reactor include the total reactivity and the reactor thermal power, the average fuel and graphite temperatures, and the helium coolant temperature, as functions of time in the simulated transients.

The performed reactivity insertion transient of the NGNP reactor follows a steady-state operation at 600 MW_{th}. At this thermal power, the calculated steady-state average fuel and graphite temperatures of $T_f^o = 1160$ K and $T_G^o = 1127.4$ K, respectively, are in good agreement with those reported by MacDonald et al. (2003), 1164 K and 1114 K, respectively, for the same helium coolant mass flow rate of 226.6 kg/s and inlet temperature of 763 K. With these helium coolant flow rate and inlet temperature in the reactor core held constant, the simulated reactivity insertion and the reactor startup transients are performed.

Based on the successful demonstration of the present PK model, it has been incorporated into MELCOR-H_2 nuclear reactor analysis code (Rodriguez et al., 2007) to simulate transient operation of a Very High Temperature Reactor (VHTR), for electricity generation, using a closed Brayton Cycle turbomachinery, and the co-generation of hydrogen using Sulfur Iodine (SI) thermochemical processes. The model could also be used for dynamic simulations of other reactor types, using the applicable reactivity feedbacks and kinetics parameters.

Acknowledgments

This research was partially funded by Sandia National Laboratories (SNL) Directed Research and Development Award Number 474270, SNL Hydrogen Generation Project-Task 80568/01 and by the University of New Mexico's Institute for Space and Nuclear Power Studies.

Nomenclature

{A}	7×7 matrix of 6-point kinetics, linear differential equations
C_i	concentration of ith group delayed-neutron precursors (atoms/m^3)
f_i	relative abundance of ith group delayed neutrons, $f_i = \beta_i/\overline{\beta}$
k	effective multiplication factor of neutron population
M	location point or vector, [x, y, z]
N, n	Neutron density (n/m^3)
P	reactor thermal power (W)
Q_f	immediate (prompt and delayed) energy released per fission (J), ~190 MeV
S	total neutron source density (n/m^3 s)
[S]	source vector (7 components)
S_o	active neutron source density (n/m^3 s)
s'_o	active neutron source (n/s)
S_o	rate of thermal power generated by active neutron source (W/s)
t	time (s)
T	temperature (K)
$\overline{T}$	volumetric average temperature (K)
v	one-group neutron speed (m/s)
VOL	volume of homogenous reactor core (m^3)
Y_i	fission power generated by ith group delayed-neutron precursors (W)

Greeks

α_j	mass fraction of graphite in zone j
β_i	effective delayed-neutron yield for the ith group
$\overline{\beta}$	total effective delayed-neutron yield, $\overline{\beta} = \sum_{i=1}^{6} \beta_i$
Δt	numerical time step size (s)
θ	implicit numerical discretization parameter, $0 < \theta < 1$
Λ	Neutron generation time (s), $\Lambda = (\nu\nu\Sigma_f)^{-1}$
λ_i	decay constant for ith delayed-neutron group (s^{-1})
ν	average number of neutrons produced per thermal fission
ρ	nuclear reactor reactivity, $\rho = 1 - 1/k$
Σa	macroscopic absorption cross-section (m^{-1})
Σf	macroscopic fission cross-section (m^{-1})
Φ	Neutron flux (n/m^2 s)
$\Psi 1$	fundamental shape mode of neutron flux (dimensionless)
[ψ]	thermal powers vector (7 components)

Subscript/Superscript

D	Doppler broadening
ext	external reactivity
f	fuel compact density feedback
G	graphite (moderator and reflector) density feedback
n	older time step value
n+1	new time step value
o	initial value at time, $t = 0$

Operators

[S]	vector (7 components)
{A}	matrix (7×7)
$\{A\}^{-1}$	inverse of matrix {A} (7×7)
{exp(A)}	7×7 exponential matrix of matrix {A}
$\{\Im\}$	7×7 Identity matrix
•	matricial and vectorial multiplication operator

References

Baker Jr., G.A., 1975. Essentials of Padé Approximants. Academic Press, Inc., New York, NY, pp. 193–205. Chapter 1, pp. 3–12, and Chapter 14.

El-Genk, M.S., Tournier, J.M., 2008. "On the use of noble gasses and binary mixtures as reactor coolants and CBC working fluids. J. *Energy Convers. Manag.* 49 (7), 1882–1891.

El-Genk, M.S., Tournier, J.-M., 2009. Effects of working fluid and shaft rotation speed on the performance of HTR plants and the size of CBC turbo-machine. J. Nucl. Eng. Des. 239, 1811–1827.

El-Genk, M.S., Tournier, P.J.-M., 2010. "On the performance of VHTR plants with direct and indirect closed Brayton cycles. ASME J. *Eng. Gas Turbine Power* 132, 0329021–0329027.

Frobenius, G., 1881. Ueber Relationen zwischem den Näherungsbrüchen von Potenzreihen. J. für die reine und angewandte Math. (Crelle's J. 90, 1–17.

Ganapol, B.D., 2013. A highly accurate technique for the solution of the non-linear point kinetics equations. Ann. Nucl. Energy 62, 564–571.

Gauntt, R.O., Cole, R.K., Erickson, C.M., Gido, R.G., Gasser, R.D., Rodriguez, S.B., Young, M.F., 2000. MELCOR Computer Code Manuals, Vol. 2: Reference Manuals, Version 1.8.5, May 2000, Report No. NUREG/CR-6119, Vol. 2, Rev. 2, SAND2000–2417/2. Sandia National Laboratories, Albuquerque, NM. October 2000.

Gill, S., 1951. A process for the step-by-step integration of differential equations in an automatic digital computing machine. In: Proceedings of the Cambridge Philosophical Society, 47. Cambridge University Press, pp. 96–108.

Goldstein, R., Shotkin, L.M., 1969. Use of the prompt-jump approximation in fast-reactor kinetics. Nucl. Sci. Eng. 38, 94–103.

Golub, G.H., van Loan, C.F., 1984. Matrix Computations, second ed. The Johns Hopkins University Press, Baltimore and London.

Greenspan, H., Kelber, C.N., Okrent, D. (Eds.), 1968. Computing Methods in Reactor

Physics. Gordon and Breach Science Publishers, Inc., New York, NY, pp. 444–506. Chapter 6.
IAEA, 2001. Current Status and Future Development of Modular High Temperature Gas Cooled Reactor Technology. International Atomic Energy Agency, Vienna, Austria. Report No. IAEA-TECDOC-1198, February 2001.
Keepin, G.R., 1965. Physics of Nuclear Kinetics. Addison-Wesley Publishing Company, Inc, Reading, Massachusetts, pp. 73–129. Chapter 4.
Keepin, G.R., Cox, C.W., 1960. General solution of the reactor kinetic equations. Nucl. Sci. Eng. 8, 670–690.
Kinard, M., Allen, E.J., 2004. Efficient numerical solution of the point kinetics equations in nuclear reactor dynamics. Ann. Nucl. Energy 31, 1039–1051.
MacDonald, P.E., Sterbentz, J.W., Sant, R.L., Bayless, P.D., Schultz, R.R., Gougar, H.D., Moore, R.L., Ougouag, A.M., Terry, W.K., 2003. NGNP Preliminary Point Design – Results of the Initial Neutronics and Thermal-Hydraulic Assessments during FY-2003. Idaho National Engineering and Environmental Laboratory, Idaho Falls, Idaho. Report No. INEEL/EXT-03–00870, Revision 1, September 2003.
MacDonald, P.E., Bayless, P.D., Gougar, H.D., Moore, R.L., Ougouag, A.M., Sant, R.L., Sterbentz, J.W., Terry, W.K., 2004. The next generation nuclear plant – insights gained from the ineel point design Studies. In: *2004 International Congress on Advances in Nuclear Power Plants (ICAPP '04), Embedded International Topical Meeting, 2004 American Nuclear Society Annual Meeting*, Held in Pittsburgh, PA, June 13-14, 2004, Paper 3405.
Mamieh, S.D., Saidinezhad, M., 2012. Analytical solution of the point reactor kinetics equations. Ann. Nucl. Energy 42, 148–152.
MatLab, 2004. MATLAB® 7.0.1. http://www.mathworks.com/products/matlab.
Nahla, A.A., Zayed, E.M.E., 2010. Solution of the nonlinear point nuclear reactor kinetics equations. Prog. Nucl. Energy 52, 743–746.
Padé, H., 1892. Sur la répresentation approchée d'une fonction par des fractions rationelles, Thesis. Ann. Ecole Nor. 9 (3), 1–93 supplement.
Porsching, T.A., 1966. Numerical solution of the reactor kinetics equations by approximate exponentials. Nucl. Sci. Eng. 25, 183–188.
Quintero-Leyva, B., 2008. CORE: a numerical algorithm to solve the oint kinetics equations. Ann. Nucl. Energey 35, 2136–2138.
RELAP5-3D Code Development Team, 2012. RELAP5-3D Code Manual Volume IV: Models and Correlations, Technical Report INEEL-ext-98-00834, Rev. 4.0.
Rodriguez, S.B., El-Genk, M.S., 2010. Numerical investigation of potential elimination of 'hot streaking' and stratification in VHTR lower plenum using helicoid inserts. J. Nucl. Eng. Des. 240, 995–1004.
Rodriguez, S.B., et al., 2007. Development of Design and Simulation Model and Safety Study of Large-scale Hydrogen Production Using Nuclear Power, Technical Report SAND2007-6218. Sandia National Laboratories, Albuquerque, NM.
Rodriguez, S.B., Louie, D., Gelbard, F., El-Genk, M.S., Gauntt, R.O., Tournier, J.-M., Cole, R., Gelbrad, F., McFadden, K., Revankar, S.T., Vierow, K., Drennen, T., Martin, B., Espinoza, F., Archuleta, L., 2009. Transient analysis of sulfur-iodine Cycle experiments and very high temperature reactor simulations using MELCOR-H2. J. Nucl. Technol. 166 (1), 76–85.
Shampine, L.F., Reichelt, M.W., 1997. The matlab ode suite. SIAM J. Sci. Comput. 18 (1), 1–22.
Shampine, L.F., Reichelt, M.W., Kierzenka, J.A., 1999. "Solving Index–I DAEs in matlab and simulink. SIAM Rev. 41 (3), 538–552.
Simulink, 2004. SIMULINK® 6.1. http://www.mathworks.com/products/simulink.
Tournier, J.-M., El-Genk, M.S., 2009. Axial flow, multi-stage turbine and compressor models. J. Energy Convers. Manag. 51, 16–29.
Travis, B.W., El-Genk, M.S., 2013. Thermal-hydraulics analyses of 1/6 prismatic VHTR core and fuel element with and without bypass flow. J. Energy Convers. Manag. 67, 326–341.
Van Loan, C., 1977. On the limitation and application of Padé approximation to the matrix exponential. In: Saff, E.B., Varga, R.S. (Eds.), Padé and Rational Approximation – Theory and Applications. Academic Press, Inc., New York, NY, pp. 439–448.
Ward, R.C., 1977. Statistical roundoff error analysis of a Padé algorithm for computing the matrix exponential. In: Saff, E.B., Varga, R.S. (Eds.), Padé and Rational Approximation – Theory and Applications. Academic Press, Inc., New York, NY, pp. 449–460.
Zhang, Z., Wu, Z., Wang, D., Xu, Y., Sun, Y., Li, F., 2009. Current status and technical description of chinese 2 x 250 MWth htr-pm demonstration plant. J. *Nucl. Eng. Des.* 239 (7), 1212–1219.